Eur. J. Mech., B/Fluids, **17,** n° 1, 79-104, 1998

Unsteady gaseous flows in rectangular microchannels: frequency response of one or two pneumatic lines connected in series

S. COLIN, C. AUBERT and R. CAEN *

ABSTRACT. – This paper represents an initial analysis of unsteady gaseous flows in a rectangular microchannel under usual pressure and temperature conditions. The effect of depth and aspect ratios of the cross-section is investigated.

With most fluid-based mechanical microsystems of small internal dimensions and subject to normal pressure and temperature conditions, flow is rarefied with slip at the walls. This flow is then modeled by the Navier-Stokes equations combined with slip and temperature jump conditions at the walls. These conditions are represented by Maxwell-Smoluchowski first order equations. By concentrating essentially on the pulsed sinusoidal regime, it is shown that the instantaneous flow rate amplitude, as well as the band pass of the microchannel are underestimated when slip at the walls is not taken into account. The frequency response of two microchannels connected in series with different cross-sectional areas is also studied. Finally, the proposed model can serve as a tool giving information about the current feasibilities of pressure sensors for the measurement of the dynamic characteristics of gaseous flows in microchannels. © Elsevier, Paris.

Keywords: Microfluidics, slip flow, frequency behavior.

1. Introduction

1.1. FLOWS IN MICROSYSTEMS

The microsystem concept appeared in the eighties, following the perfecting of surface micro-machining techniques on silicon wafers. The idea of associating sensors, actuators, signal and energy processing components on a silicon substratum, perfectly compatible with microelectronics, has since made significant progress.

The development of microfluidics (concerned with microsystems which use or transport fluids) has been particularly striking during the past 10 years. Microfluidic devices, relatively rare in 1990 (Van de Pol and Branebjerg, 1990), are now increasingly used. Gravesen *et al.* (1993) and Shoji and Esashi (1994) have written two reviews of basic microfluidic components (microvalves, micropumps, mass flow microsensors,

* Laboratoire de Génie Mécanique de Toulouse, INSAT, Complexe Scientifique de Rangueil, 31077 Toulouse Cedex 04, France.

E-mail: stephane.colin@gmm.insa-tlse.fr

E-mail: cecile.aubert@gmm.insa-tlse.fr

E-mail: robert.caen@gmm.insa-tlse.fr

0997-7546/98/01/© Elsevier, Paris

microamplifiers,...) as well as more complex fluid microsystems (such as mechanical dosing systems or integrated chemical analysis systems). At that time, efforts were concentrated on the making rather than the modeling of these various devices. This modeling was still often rudimentary and mainly concerned incompressible flows (Zengerle and Richter, 1994). Since 1994, numerous papers have presented new microfluidic devices, devoting considerable time to modeling and the integration of flow simulation in the complete microsystem model. To achieve this aim, standard simulators for cross-disciplinary system approaches have been used e.g. FLOTRAN (Schomburg *et al.*, 1994), SPICE (Bourouina and Grandchamp, 1996) and PSPICE (Carmona *et al.*, 1996).

However, these different studies fail to take into account the effect of scale of the devices on gaseous flows. This has since been the origin of several experimental as well as theoretical studies of gaseous flows in microchannels, the basic elements in microfluidics. The choice of silicon as the standard basic material for microsystems leads to microchannels with rectangular cross-sections, if they are milled by the LIGA process (Schomburg *et al.*, 1994). With more conventional processes such as photolithography, the cross-sections are trapezoidal, but generally remain close to rectangular sections, the depths being often very small compared to the widths. One can first observe that for a liquid flow, the more challenging problems are those linked to surface forces. For example, the presence of gas bubbles plays a significant role, as surface tensions increase, due to the high curvature of the interfaces. This is a problem both for the modeling and the operating of the microsystems as well as for interfacial effects such as interfacial electric double layer (EDL) which cannot be neglected in modeling heat transfer of liquid flows in microchannels (Mala *et al.*, 1997). On the other hand, these effects vanish in the case of gas flows. The only problems due to surface forces appear when wall roughness may not be considered as negligible compared with the cross-dimensions of the channel. The influence of surface roughness, when not negligible, has been studied by several authors, for example Sugiyama *et al.* (1996) and Chu (1996). However, as the shallower microchannels are generally micromachined by plasma etching, the surface roughness typically obtained is always less than 1% for a .5 μm deep channel (Harley *et al.*, 1995): the maximum peak-valley is 4.88 nm. So, the distinctive features of usual gaseous flows in microchannels are mainly the shape of the section (rectangular), rarefaction and unsteadiness. Indeed, with cross-dimensions typically of the order of 1 μm and with pressure and temperature approaching atmospheric conditions, the Knudsen number, which is the ratio of the mean free path over a characteristic dimension, ranges from .01 to .1. In this range, the flow is called slip flow and can be modeled by the Navier-Stokes equations supplemented by slip and temperature jump conditions at the walls. In the conventional analysis, velocity slip at the walls is assumed to be proportional to the normal velocity gradient. The same is true of the temperature jump and the temperature gradient respectively. This assumption is valid if the velocity and temperature profiles are essentially linear over a mean free path. It leads to the Maxwell-Smoluchowski boundary conditions, which are therefore of the first-order (Kennard, 1938). Second-order slip conditions have been obtained since 1947, and later improved, notably by Deissler

(1964). These enable the range of applicability of the slip flow theory to be extended to higher Knudsen numbers. Moreover, as microfluidic devices (*i.e.* micropumps) essentially work under a pulsed regime, it is necessary to consider unsteady flows in microchannels. State of the art research into these two main points (rarefaction and unsteadiness), in connection with gaseous flows in rectangular microchannels, is summarized in the following two paragraphs.

1.2. Rarefaction effects

A general review on rarefied gas dynamics has been given by Muntz (1989).

The first analytical results concerning steady slip flows in long ducts were published in the thirties. As an example, Kennard (1938) gave a simple expression for the mass flow rate through a long circular pipe, and also - per unit of width - through a parallel-plate channel. This solution consists of a correction to Poiseuille's formula, therefore assuming an incompressible and fully developed steady flow, with first-order slip conditions at the walls. Heat transfer in microtubes has also been investigated by Barron *et al.* (1997), who evaluated the eigenvalues for the Graetz problem in slip flow. The Graetz problem is a simplified case of the problem of forced convection heat transfer in a circular tube in laminar flow, assuming steady and incompressible flow, constant fluid properties, no 'swirl' component of velocity, fully developed velocity profile and negligible energy dissipation effect. Thomson and Owens (1975) have presented a survey of internal rarefied flows, focusing on the analytical determination of the flow rate through infinite circular tubes. In particular, they were interested in the empirical methods used to provide a smooth transition from slip to molecular flow. They pointed out that slip theory contains the inherent error that flow remains unchanged as the Knudsen number is increased and showed that the concept of specular reflection accurately approximates the wall boundary condition. As far as we are aware, only Ebert and Sparrow (1965) have modeled steady flow of a gas in rectangular channels with slip conditions at the wall, but without experimental comparisons. The analytical solution they obtained, using Fourier series expansions, shows that the effect of slip is to flatten the velocity distribution relative to that for a continuum flow. Moreover, the axial pressure gradient is diminished under slip conditions. Lastly, Ebert and Sparrow showed that compressibility (only taken into account in an approximate analysis, assuming locally fully developed and isothermal flow) increases the pressure drop primarily through an increase in viscous shear rather than an increase in momentum flux. Moreover, the same conclusions are qualitatively valid for slip flows in annular ducts.

More recently, several works based on a numerical approach and dealing with rarefied gas flows in channels have been published. Stefanov and Cercignani (1994) have tried to bring to the fore the transition to turbulence for a monatomic rarefied flow in a channel. For this, they used the Direct Simulation Monte Carlo Method (DSMC), solving Boltzmann's equation combined with a diffuse reflection on the walls. The flow was due to body forces applied in the direction parallel to the walls and acting on each gas molecule. The Knudsen number ranged from .005 to .1. However, the study of the transition was incomplete, as calculations were intrinsically two-dimensional. By also

using the DSMC, Sone *et al.* (1996) studied the behavior of a steady one-way flow of a rarefied gas induced by a periodic temperature distribution along a channel and without any applied pressure gradient. The channel consisted of two parallel plates on which a series of ditches was dug at equal spaces. The behavior of the rarefied gas was investigated numerically for various Knudsen numbers. The recent work of Piekos and Breuer (1996) deals more specifically with microflows, giving details of a DSMC investigation of flows related to microelectromechanical systems (MEMS). The first case explored with their code was a steady, low speed, slip flow of nitrogen through a 31.14 × 1.04 μm channel. This canonical case was tested with the purpose of validating the algorithm. A very close correlation between numerical results and theoretical predictions has been obtained. The second case explored was a flow of nitrogen through a 6.61 × .11 μm channel. The Knudsen numbers ranging from .1 to 3, this case was relevant to the transition regime. A comparison between numerical and theoretical predictions of pressure distribution has confirmed that for these Knudsen numbers, the slip theory began to fail. So, the DSMC was also used for determining the Knudsen limit (about .15) of the slip theory. At the same time, Beskok *et al.* (1996) developed the spectral element code "μFlow", which aims to analyze rarefaction, compressibility, viscous heat and thermal creep effects on a steady rarefied gas flow. In a previous paper, Beskok and Karniadakis (1994) dealt with an incompressible flow model with high order slip velocity. In the latest paper, the authors propose a numerical, compressible, no-slip as well as slip flow formulation with second-order slip velocity. They compare their numerical results with experimental data and analytical models of the literature for microflows between two parallel plates. However, their numerical models are also appropriate for complex geometries, such as grooved microchannels. The main conclusions are the following. Firstly, the use of a first-order slip-flow boundary condition, neglecting higher orders, leads to the increase in mass flow rate – due to slip at the walls – being overestimated. Secondly, as regards pressure-driven flows, it is shown that rarefaction negates compressibility, which tends to create a non-linear pressure distribution. Lastly, for shear-driven flows, it is shown that compressibility effects are negligible, drag being essentially reduced by rarefaction, and that viscous heating effects generate significant temperature gradients in microsystems even for isothermal boundary conditions.

Concerning the experimental approach, Sreekanth (1968) has examined the rarefied flow of nitrogen gas through long circular tubes, measuring the mass flow, pressure drop and cross-sectional velocity profiles. He has shown that the slip flow theory (with isothermal and locally fully developed flow assumptions) correlates closely with experimental data until the Knudsen number reaches a value of about .13. Comparisons between experiment and theory using second-order boundary conditions have also been made. Whereas the tubes used by Sreekanth had large diameters (2 inches), more recent studies concern microflows. Tison (1993) has measured gas flows through stainless steel capillary tubes, about 1 μm in diameter, for a large range of the Knudsen number that may achieve values up to 200. The flow rate is very accurately predicted by the slip flow equation, particularly for crimped capillaries. Other experimental studies concern flow in rectangular microchannels on silicon wafers. The first measurements (Choi *et al.*, 1991, Pfahler *et al.*,

1991) were restricted to the flow rate and the pressure drop between the inlet and the outlet. Subsequently, Pong *et al.* (1994) proposed an experimental set-up to measure the non-linear pressure distribution along a microchannel. A series of pressure sensors, 250 by 250 μm^2 in area, was connected to a 1.2 μm deep channel through a 2 μm by .3 μm bridging channel. Both helium and nitrogen as working fluids were used. The authors concluded that the non-linear pressure distribution was affected by viscous heat and by the Knudsen number variations. Arkilic *et al.* (1994) have compared their experimental data for a 1.33 μm deep and 52.25 μm wide microchannel with an analytical slip flow model of a steady flow between two parallel plates. For a Knudsen number of between .003 to .2, experimental results correlated closely to theoretical predictions assuming isothermal, locally fully developed flow. It was shown that the slip boundary condition reduces the axial pressure gradient, consequently increasing flow rate compared to a flow in which slip is considered as negligible. Similarly, Harley *et al.* (1995) observed that experimental data were within 8% of theoretical predictions assuming isothermal, locally fully developed, first-order, slip flow. In their experiment, the Knudsen number was less than .38. Since the aspect ratio of microchannels in question was small, experimental results were also compared with a model of slip flow between two parallel plates.

1.3. Unsteadiness effects

With regard to unsteady flows of gases in uniform channels, several theoretical and experimental studies of frequency response of pneumatic lines were published during the sixties. Nichols (1962) modeled unsteady compressible ideal gas flow through a circular tube, but without experimental comparison. The temperature of the walls was supposed to be constant and pressure was assumed to be uniform within the cross-section. In addition, the sole component of velocity taken into account was along the axis of the tube. Under a pulsed sinusoidal regime, the velocity solution was expanded in terms of Bessel functions. Later, D'Souza and Oldenburger (1964) published experimental data obtained from frequency-response tests for liquids in a circular tube. A matrix relation between pressure and velocity amplitudes for channels with small diameter was established. Under a pulsed sinusoidal regime, the velocity solution in terms of Bessel functions was also proposed. In conclusion, close correlation between experiments and theory was observed. As regards gaseous flows in rectangular channels, Schaedel (1968) proposed a model based on same flow assumptions as those employed by Nichols, but in which the velocity solution is expanding in terms of the Fourier series. Finally, Healey and Carlson (1969) compared Schaedel's and Nichols' models with an equivalent hydraulic mean diameter by studying experimentally the frequency response of rectangular channels. For a .7 mm deep channel, close correlation between experiment and both theories was observed. For a .5 mm deep channel, experimental results corresponded closely to Schaedel's model, but Nichols' model with an equivalent hydraulic mean diameter contained some deviations compared with experiments. The non-linear terms in the continuity and momentum equations, which may not be neglected for large pressure fluctuations, were taken into account by Funk and Robe (1969). A number of other experimental and theoretical studies of the frequency response of pneumatic lines were made during the heyday of fluidics.

The main models have been summarized in White's textbook (1991). But as far as we know, the smallest depth encountered was of the order of .5 mm. For such a dimension, flow can be considered as a continuum. Unfortunately, in the literature, very little work is reported on unsteady slip flow. Norberg *et al.* (1997) have experimentally studied transient flows in microchannels with a mass spectrometric system, but for very low transients (of the order of 10 seconds) and in the molecular regime. Bestman *et al.* (1995) have considered the Rayleigh problem for slip flow. Arkilic and Breuer (1993) have modeled an unsteady microflow induced by oscillating plates. But since their primary interest was the study of viscous losses due to the oscillating surface, the governing equation only represented a balance between the unsteady and viscous forces. Lately, Caen *et al.* (1996) presented a model of a pulsed slip flow in microtubes but only with circular cross-section.

The aim of the present paper is therefore to propose a theoretical model for unsteady gas flow in rectangular microchannels (pneumatic microlines) induced by small pressure fluctuations. In order to show the influence of slip on the instantaneous velocity profile and on the frequency response of a microline, a simple analytical model of the flow is proposed, which could be easily used in a cross-disciplinary system approach for analysing microsystems. As one of the future goals is to control the behavior of microsystems (micropumps, micro mixers, chromatographs, micro dosing systems,...) connecting several microchannels of different sizes, we have initially studied the simplified case of two lines connected in series.

2. Method and assumptions

Let us consider a pneumatic line with a uniform rectangular cross-section (Σ). The depth and the width of the cross-section are respectively denoted by $2\,h$ and $2\,b$ in Figure 1 The Cartesian coordinates with the origin located in the center of the cross-section are used.

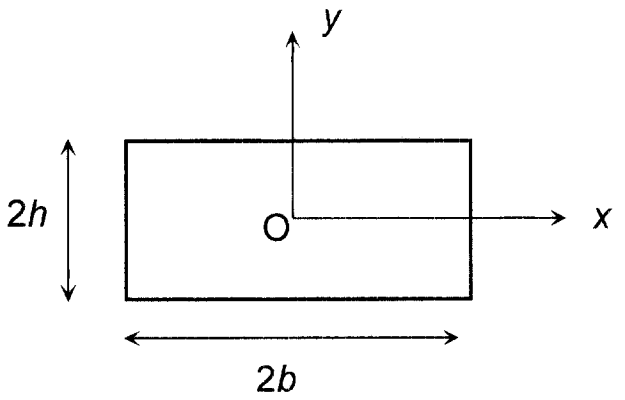

Fig. 1. – Cross-section of the microchannel.

The aspect ratio of the cross-section is denoted by a and defined as

$$a = \frac{h}{b}. \tag{1}$$

Without restricting the problem, the depth $2h$ of the microchannel is chosen as the smallest dimension and the width $2b$ of the microchannel as the largest dimension of the cross-section (Σ). Consequently, $0 < a \leq 1$.

The Knudsen number Kn is defined as the ratio

$$Kn = \frac{\lambda}{D_h} = \frac{\lambda(1+a)}{4h}. \tag{2}$$

where λ is the molecular mean free path and D_h the hydraulic diameter.

The following study is designed to demonstrate the influence of slip on the instantaneous velocity profiles within a given cross-section, and then on the frequency response of the line. A sinusoidal pressure fluctuation is generated at the inlet of the pneumatic line and the dynamic response of this line whether slip at the walls is taken into account or not, is studied. With this in mind, a model of unsteady slip flow will be compared to a model without slip at the walls. This no-slip model corresponds to a continuum regime, like that encountered in lines whose dimensions are of the order of one millimeter under usual pressure and temperature conditions.

Section 3 describes the instantaneous velocity profile within a cross-section. The behavior of one uniform pneumatic line and that of two pneumatic lines connected in series, each of whose cross-section is uniform, are presented in sections 4 and 5 respectively.

The following assumptions have been made:

– the flow under consideration is assumed to be laminar and to behave as an ideal gas.

The shear viscosity and thermal conductivity are assumed constant.

– the gas is initially at rest and then subjected to small pressure fluctuations. Each variable (pressure, density, temperature and velocity) may be written as follows: $\bar{g}(x, y, z) + g(x, y, z, t)$. The fluctuations g are supposed small compared with the mean values $\bar{g}$ for the pressure, the density and the temperature. Besides, since the gas is initially at rest, the problem can be dealt without coupling of temperature and velocity. However, expression of fluctuating temperature is necessary to model the frequency response of a pneumatic line in sections 4 and 5.

– the lines in question are rigid ducts with rectangular cross-section whose axial dimension L along z is much higher than those along x and y, namely $2b$ and $2h$.

– the fluctuating flow is supposed parallel to the z-axis, that is, a plane wave hypothesis is made. The sole z component of velocity is denoted by w. This is justified by previous works concerning the frequency response of rectangular channels, with dimensions of the order of one millimeter. See for example the paper of Healey (1969).

– the fluctuating pressure is constant within the cross-section. This assumption has been justified by Harley *et al.* (1995) for a steady compressible flow between two parallel plates. They have shown that the transverse velocity could be neglected and the pressure and density could be assumed uniform within the cross-section. Their experimental results have confirmed the theoretical predictions.

As a result of the previous assumptions, the fluctuating gas flow must satisfy the following continuity, momemtum balance, energy conservation and state equations:

$$\frac{\partial \rho}{\partial t} + \frac{\partial (\bar{\rho} w)}{\partial z} = 0, \tag{3}$$

$$\frac{\partial^2 w}{\partial x^2} + \frac{\partial^2 w}{\partial y^2} - \frac{\bar{\rho}}{\mu} \frac{\partial w}{\partial t} = \frac{1}{\mu} \frac{\partial p}{\partial z}, \tag{4}$$

$$\frac{\partial^2 \tau}{\partial x^2} + \frac{\partial^2 \tau}{\partial y^2} - \frac{\sigma \bar{\rho}}{\mu} \frac{\partial \tau}{\partial t} = -\frac{\sigma}{\mu C_p} \frac{\partial p}{\partial t}, \tag{5}$$

$$p = r (\bar{\rho} \tau + \rho \bar{\tau}), \tag{6}$$

in which ρ, p, τ are respectively the fluctuations of density, pressure and temperature. C_p denotes the specific heat at constant pressure; $\bar{\tau}$ and $\bar{\rho}$ represent the gas temperature and density at rest; μ denotes the shear viscosity, r the gas constant and t the time variable; σ denotes the Prandtl number and is defined by:

$$\sigma = \frac{\mu C_p}{k}, \tag{7}$$

where k is the coefficient of thermal conductivity. Note that the assumption that the gas is initially at rest, enables the divergence term $\bar{w} \frac{\partial w}{\partial z}$ to be eliminated, since $\bar{w} = 0$.

3. Fluctuating velocity profiles within a cross-section

A modeling of the instantaneous velocity profile within a given cross-section (defined by z) of a microchannel and under a pulsed sinusoidal regime is presented here.

3.1. Modeling

The local slip velocity is assumed proportional to the local velocity gradient normal to the wall and the boundary conditions in terms of velocity are expressed by the Maxwell equations

$$w|_{y=h} = -\kappa\lambda \left[\frac{\partial w}{\partial y}\right]_{y=h}, \qquad w|_{x=b} = -\kappa\lambda \left[\frac{\partial w}{\partial x}\right]_{x=b}, \tag{8a, b}$$

whereas the symmetry of the problem with respect to the x and y-axes implies

$$\left[\frac{\partial w}{\partial y}\right]_{y=0} = 0, \qquad \left[\frac{\partial w}{\partial x}\right]_{x=0} = 0. \tag{8c, d}$$

These symmetries enable the study to be restricted to the quadrant $0 \leq x \leq b$ and $0 \leq y \leq h$.

The mean free path λ can be expressed for an ideal gas by:

$$\lambda = \frac{\mu}{\bar{\rho}} \sqrt{\frac{\pi}{2\, r\, \bar{\tau}}} \tag{9}$$

and $\kappa = \kappa_0 \frac{2-\xi}{\xi}$. The coefficient κ_0 is a constant, lying between 0.982 and 0.998, so very nearly unity. ξ denotes Maxwell's specular reflection coefficient which depends on surface roughness and type of gas. This coefficient ξ, verifying $\xi < 0 \leq 1$, is the fraction of the molecules' tangential momentum lost through collisions with the walls. In his book, Schaaf (1963) has reported values of ξ, ranging from .6 to 1, as a function of the nature of the gas and the type of the surface. Albertoni *et al.* (1963) have calculated $\kappa = 1.1466$ which is accurate to the fourth decimal figure. This result was obtained by solving numerically the linearized Boltzmann equation. Sreekanth (1968) was interested in experiments on steady rarefied nitrogen flow in circular tubes. For $Kn \leq .03$, a close correlation between theory and experimental results was observed for either $\kappa = 1$ or $\kappa = 1.1466$. For $Kn < .05$, the closest correlation for $\kappa = 1$ was noted. Finally, for $Kn > .05$, the closest correlation occurred for $\kappa = 1.1466$. In conclusion, the value of κ not only depends on surface roughness but also on the Knudsen number.

After performing a Laplace transform, the momentum Eq. (4) becomes:

$$\frac{\partial^2 \widetilde{W}}{\partial x^2} + \frac{\partial^2 \widetilde{W}}{\partial y^2} - \frac{s\,\bar{\rho}}{\mu} \widetilde{W} = \frac{1}{\mu} \frac{\partial \widetilde{P}}{\partial z}, \tag{10}$$

in which s is the Laplace variable corresponding to the time variable t, and $\widetilde{W}$ and $\widetilde{P}$ are the Laplace transforms of the velocity w and pressure p.

At this stage, it is convenient to introduce dimensionless coordinates

$$x^* = \frac{x}{b}, \qquad y^* = \frac{y}{h}, \qquad z^* = \frac{z}{L}. \tag{11}$$

Thus, the momentum balance Eq. (10) and boundary conditions (8a-d) become:

$$a^2 \frac{\partial^2 \widetilde{W}}{\partial x^{*2}} + \frac{\partial^2 \widetilde{W}}{\partial y^{*2}} - \omega_{r'} \widetilde{W} = \frac{h^2}{\mu L} \frac{\partial \widetilde{P}}{\partial z^*}, \tag{12}$$

$$\widetilde{W}|_{y^*=1} = -2\,\kappa\, K \left[\frac{\partial \widetilde{W}}{\partial y^*}\right]_{y^*=1}, \qquad \widetilde{W}|_{x^*=1} = -2\,a\,\kappa\, K \left[\frac{\partial \widetilde{W}}{\partial x^*}\right]_{x^*=1}, \tag{13a, b}$$

$$\left[\frac{\partial \widetilde{W}}{\partial y^*}\right]_{y^*=0} = 0, \qquad \widetilde{W}|_{x^*=1} = -2\,a\,\kappa\, K \left[\frac{\partial \widetilde{W}}{\partial x^*}\right]_{x^*=1}, \tag{13c, d}$$

where

$$\omega_{r'} = \frac{s\,\bar{\rho}\,h^2}{\mu}. \tag{14}$$

The depth of the microchannel being substituted for the hydraulic diameter, the dimensionless parameter K actually defines another Knudsen number distinct from the one introduced in Eq. (2):

$$K = \frac{\lambda}{2h} = \frac{2Kn}{1+a}. \tag{15}$$

A solution for the axial velocity may be proposed as follows:

$$\widetilde{W}(x^*, y^*, s) = \sum_{i=1}^{\infty} F(x^*, b_i, s) \cos(b_i y^*). \tag{16}$$

The condition (13a) requires b_i to be solutions of the equation

$$b_i \tan b_i = \frac{1}{2K\kappa}. \tag{17}$$

In order to determine the function $F(x^*, b_i, s)$, solution (16) is substituted into the momentum Eq. (12). Furthermore, the right-hand side is expanded in series in terms of the orthogonal functions $\cos(b_i y^*)$. The function $F(x^*, b_i, s)$ is entirely determined by the conditions (13b) and (13d).

Finally, the form of the velocity distribution $\widetilde{W}$ follows as:

$$\widetilde{W}(x^*, y^*, s) = -2\frac{h^2}{\mu L}\frac{\partial \widetilde{P}}{\partial z^*} \sum_{i=1}^{\infty} \frac{\sin(b_i)\cos(b_i y^*)}{b_i(1+\Phi \sin^2(b_i))(b_i^2+\omega_{r'})} d_i, \tag{18}$$

with

$$d_i = 1 - \frac{\cosh\left(\sqrt{b_i^2+\omega_{r'}}\,\frac{x^*}{a}\right)}{\cosh\left(\sqrt{\frac{b_i^2+\omega_{r'}}{a}}\right) + \Phi\sqrt{b_i^2+\omega_{r'}}\sinh\left(\sqrt{\frac{b_i^2+\omega_{r'}}{a}}\right)}, \tag{19}$$

and

$$\Phi = 2K\kappa. \tag{20}$$

The solution of the fluctuating temperature τ can be obtained by a similar calculation. The Laplace transform $\widetilde{T}$ of the fluctuating temperature must obey the equations:

$$a^2\frac{\partial^2 \widetilde{T}}{\partial x^{*2}} + \frac{\partial^2 \widetilde{T}}{\partial y^{*2}} - \sigma\omega_{r'}\widetilde{T} = -\frac{\sigma}{\bar{\rho}C_p}\omega_{r'}\widetilde{P}, \tag{21a}$$

$$\widetilde{T}|_{y^*=1} - \widetilde{T}_{\text{wall}} = -\left(\frac{2-\alpha}{\alpha}\right)\frac{2\gamma}{\gamma+1}\frac{2K\kappa_0}{\sigma}\left[\frac{\partial \widetilde{T}}{\partial y^*}\right]_{y^*=1}, \tag{21b}$$

(21c) $$\tilde{T}|_{x^*=1} - \tilde{T}_{\text{wall}} = -\left(\frac{2-\alpha}{\alpha}\right)\frac{2\gamma}{\gamma+1}\frac{2aK\kappa_0}{\sigma}\left[\frac{\partial\tilde{T}}{\partial x^*}\right]_{x^*=1},$$

(21d, e) $$\left[\frac{\partial\tilde{T}}{\partial x^*}\right]_{x^*=0} = 0, \qquad \left[\frac{\partial\tilde{T}}{\partial y^*}\right]_{y^*=0} = 0.$$

The temperature-jump due to energy conservation near the walls [Eqs. (21b) and (21c)] is obtained by the Smoluchowsky condition (Schaaf, 1963). In these equations, γ represents the ratio of the specific heats and α denotes the thermal accommodation coefficient. Schaaf (1963) reported values of α as a function of surface type and temperature and nature of gas. These values range from .0109 to .99. The temperature fluctuation at the wall $\tilde{T}_{\text{wall}}$ is always assumed to be equal to zero; the thermal conductivity of silicon is large enough that the isothermal wall assumption made here correlates to most of the cases encountered in reality.

By the same reasoning, the solution of the fluctuating temperature distribution $\tilde{T}$ follows as:

(22) $$\tilde{T}(x^*, y^*, s) = 2\frac{\omega_{r'}\sigma}{\bar{\rho}C_p}\tilde{P}\sum_{i=1}^{\infty}\frac{\sin(c_i)\cos(c_i y^*)}{c_i(1+\phi\sin^2(c_i))(c_i^2+\sigma\omega_{r'})}g_i,$$

with

(23) $$g_i = 1 - \frac{\cosh\left(\sqrt{c_i^2+\sigma\omega_{r'}}\frac{x^*}{a}\right)}{\cosh\left(\sqrt{\frac{c_i^2+\sigma\omega_{r'}}{a}}\right) + \phi\sqrt{c_i^2+\sigma\omega_{r'}}\sinh\left(\sqrt{\frac{c_i^2+\sigma\omega_{r'}}{a}}\right)}$$

and

(24) $$\phi = \left(\frac{2-\alpha}{\alpha}\right)\frac{4\gamma K\kappa_0}{(\gamma+1)\sigma},$$

where the c_i are the solution of

(25) $$c_i \tan c_i = \frac{1}{\phi}.$$

In all the following sections, the study is restricted to the pulsed sinusoidal regime. The variable s may be thus substituted for $j\omega$ (with $j^2 = -1$) where ω represents the generating frequency. The complex velocity amplitude $W(x^*, y^*, s)$ is then obtained from Eq. (18). In the same way, the complex temperature amplitude $T(x^*, y^*, \omega)$ is obtained from Eq. (22). The complex pressure amplitude is noted $P(\omega)$.

The expression for the local reference velocity W_0 is given by:

(26) $$W_0 = \frac{-2h^2}{\mu L}\frac{\partial P}{\partial z^*},$$

and the local reference temperature T_0 by:

$$T_0 = \frac{2\sigma}{\bar{\rho} C_p} P. \tag{27}$$

Normalized solutions W^* and T^* may thus be written in the following complex form:

$$W^*(x^*, y^*, \omega) = \frac{W}{W_0} = \sum_{i=1}^{\infty} \frac{\sin(b_i)\cos(b_i y^*)}{b_i(1+\Phi\sin^2(b_i))(b_i^2 + j\omega_r)} d_i \tag{28}$$

with

$$d_i = 1 - \frac{\cosh\left(\sqrt{b_i^2 + j\omega_r}\,\frac{x^*}{a}\right)}{\cosh\left(\sqrt{\frac{b_i^2 + j\omega_r}{a}}\right) + \Phi\sqrt{b_i^2 + j\omega_r}\sinh\left(\sqrt{\frac{b_i^2 + j\omega_r}{a}}\right)}, \tag{29}$$

and

$$T^*(x^*, y^*, \omega) = \frac{T}{T_0} = j\omega_r \sum_{i=1}^{\infty} \frac{\sin(c_i)\cos(c_i y^*)}{c_i(1+\phi\sin^2(c_i))(c_i^2 + j\omega_r\sigma)} g_i \tag{30}$$

with

$$g_i = 1 - \frac{\cosh\left(\sqrt{c_i^2 + j\omega_r\sigma}\,\frac{x^*}{a}\right)}{\cosh\left(\sqrt{\frac{c_i^2 + j\omega_r\sigma}{a}}\right) + \phi\sqrt{c_i^2 + j\omega_r\sigma}\sinh\left(\sqrt{\frac{c_i^2 + j\omega_r\sigma}{a}}\right)}. \tag{31}$$

The parameter ω_r is the ratio of the generating frequency to a characteristic frequency ω_c:

$$\omega_r = \frac{\omega}{\omega_c}, \tag{32}$$

with

$$\omega_c = \frac{\mu}{\bar{\rho} h^2} = \frac{4\mu}{\bar{\rho} S a}, \tag{33}$$

where S is the area of the section (Σ).

When ω_r tends towards zero, we obtain the same expression for velocity as that found by Ebert and Sparrow (1965) for a steady rarefied gas flow in rectangular channels.

In order to evaluate Eqs. (28) and (30), it is necessary to precompute the roots b_i and c_i. The first 50 solutions of Eqs. (17) and (25) are thus determined numerically for depths of the microchannel between .62 and 10.35 μm.

3.2 Analysis

Introducing the complex pressure form $p = |P|e^{j\omega t}$ (only the real part being physically significant), the following instantaneous velocity distribution is obtained:

$$(34)\quad w^*(x^*, y^*, t) = \mathrm{Re}\,[W^* e^{j\omega t}] = \mathrm{Re}\,[W^*(x^*, y^*, \omega)\cos(\omega t)] - \mathrm{Im}\,[W^*(x^*, y^*, \omega)]\sin(\omega t)$$

So as to emphasize the influence of the Knudsen number on the instantaneous velocity profile, the results based on the foregoing slip model [Eq. (34)] are compared to a no slip model (Schaedel, 1968) which can also be obtained by taking $Kn = 0$ in our equations.

Figure 2 and 3 respectively illustrate the effect of the depth $2h$ of the microchannel and the phase ωt on the instantaneous velocity profile w^*. In these two examples, the frequency f ($f = \frac{\omega}{2\pi}$) is equal to 5000 Hz.

Figure 2 represents the slip and no-slip instantaneous velocity profiles w^* for two microchannels of different depths. These microchannels have a square cross-section with sides .62 μm and 2.07 μm respectively. For a mean pressure $\bar{p} = .11$ MPa and a mean temperature $\bar{\tau} = 293$ K, the Knudsen numbers have a value of .1 and .03 respectively. In these two cases, the phase ωt is equal to 0°. The instantaneous velocity profiles w^* are plotted as a function of the parameter y^* for a given x^*. The whole section has been studied, but for reasons of clarity, only two results at $x^* = 0$ and $x^* = .9$ are presented here. It can be seen that by not taking into account slip at the walls, the instantaneous velocity at any point in the cross-section is underestimated. Furthermore, in keeping with the results based on the steady regime, the slip increases with the Knudsen number. Finally, whether slip at the walls is taken into account or not, the instantaneous velocity profiles reach their maximum on the cross-section center line *i.e.* at $x^* = 0$.

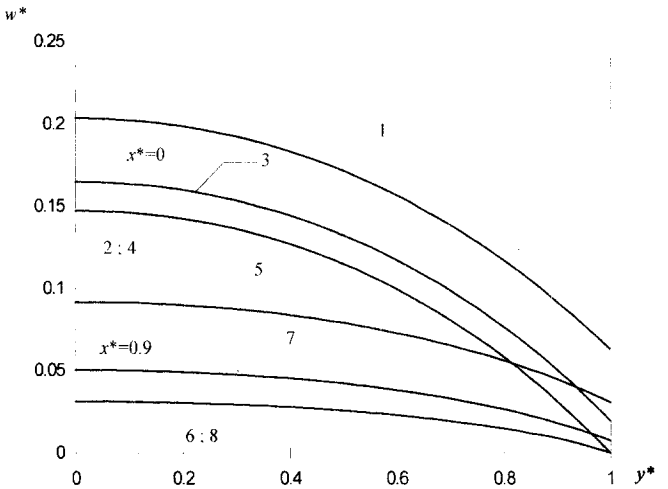

Fig. 2. – Instantaneous velocity profiles w^* within a cross-section as a function of the parameter y^* and under a pulsed sinusoidal regime. $f = 5000$ Hz, $a = 1$, $\omega t = 0°$, $\bar{\tau} = 293$ K, $\bar{p} = .11$ MPa.
$x^* = 0$: $2h = .62$ μm **1** slip flow, **2** no-slip flow. $2h = 2.07$ μm **3** slip flow, **4** no-slip flow.
$x^* = .9$: $2h = .62$ μm **5** slip flow, **6** no-slip flow. $2h = 2.07$ μm **7** slip flow, **8** no-slip flow.

Figure 3 represents the slip and no-slip instantaneous velocity profiles w^* for different values of the phase ωt and at $x^* = 0$. The microchannel in question is 1.03 μm deep with an aspect ratio .25. For the same pressure and temperature conditions as before, the Knudsen number is equal to .0375. It can be seen that the phase ωt has no influence on the shape of the profiles w^*: whatever value of the phase is chosen, the profiles are almost parabolic.

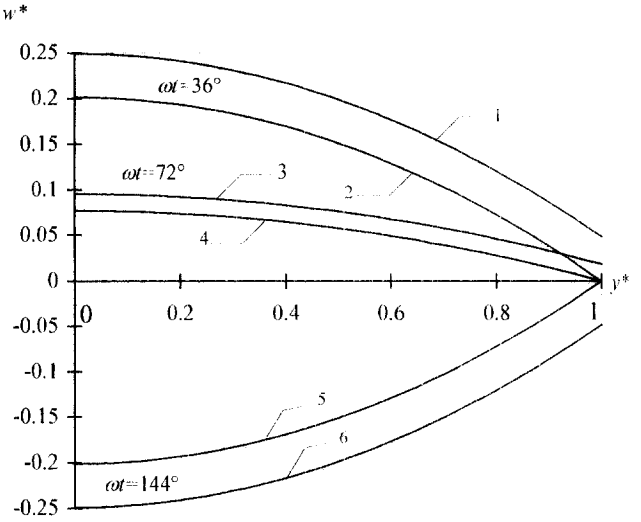

Fig. 3. – Instantaneous velocity profiles w^* within a cross-section for different values of phase ωt and under a pulsed sinusoidal regime. $x^* = 0$, $f = 5000$ Hz, $a = .25$, $2h = 1.03$ μm, $\bar{\tau} = 293$ K, $\bar{p} = .11$ MPa. $\omega t = 36°$: **1** slip flow, **2** no-slip flow. $\omega t = 72°$: **3** slip flow, **4** no-slip flow. $\omega t = 144°$: **5** slip flow, **6** no-slip flow.

These figures only represent examples of the gas behavior for a given frequency. But the trend of these profiles is representative of the behavior within a large frequency range under pressure and temperature conditions of the order of .1 MPa and 300 K respectively. A complementary computation shows that with the frequencies used, the instantaneous velocity profiles in ducts with cross-dimensions of the order of one millimeter present inflection points and reach a maximum away from the axes of the cross-section (Caen, 1979). However, such a trend appears in ducts with cross-dimensions of the order of one micrometer at much higher frequencies, of the order of 10^7 Hz and more. Moreover, from Figure 2, the individual no-slip instantaneous velocity profiles w^* are indistinguishable, whatever the microchannel depth. In contrast, the slip instantaneous velocity profiles w^* are distinct. But, whether slip at the walls is taken into account or not, the instantaneous velocity profile depends on the microchannel depth $2h$ which appears in the expression of the parameter ω_r ($\omega_r = \frac{\omega \bar{\rho}}{\mu} h^2$). Nevertheless, the depths of the microchannels in question are of the order of one micrometer and the frequency of the order of 5000 Hz. Consequently, the variable ω_r is negligible whether slip is taken into account or not. Thus, the depth $2h$ only has a significant influence on the coefficient K. Therefore, the instantaneous velocity is altered by slip. Notice also that the form of the variables under consideration leads us to use several parameters: K, ω_r, S, a. But some of these

parameters are interconnected ($K = \frac{\lambda}{2h}$, $\omega_r = \frac{f\,\pi\,S\,a\,\bar{\rho}}{2\mu}$ and $S = \frac{4h^2}{a}$), thus making it difficult to assess the individual influence of each parameter.

The present study of the instantaneous velocities enables us to verify that the instantaneous flow rate increases with slip as in the steady regime. However, in order to quantify the influence of slip on signal propagation, the frequency response of the microchannel has to be studied as well.

4. Frequency response of a pneumatic line

To ascertain the frequency response of a uniform rectangular line, we have related the inlet pressure and mass flow rate complex amplitudes to the outlet pressure and mass flow rate complex amplitudes. The reference variables at the inlet and at the outlet of the line will be denoted by e and s respectively.

4.1. Modeling

Let

$$\dot{m} = \bar{\rho} \iint_{(\Sigma)} w\,dx\,dy \tag{35}$$

be the mass flow rate through the cross-section (Σ). Under a pulsed regime, after performing a Laplace transform and integrating across the section, Eq. (3) becomes:

$$\frac{\partial \dot{M}}{\partial z} = -j\,\omega\,\frac{PS}{\bar{\tau}\,r} + j\,\omega\,\frac{\bar{\rho}}{\bar{\tau}} \iint_{(\Sigma)} T\,dx\,dy, \tag{36}$$

where $\dot{M}$ is the Laplace transform of the mass flow rate $\dot{m}$.

Likewise, by integrating Eq. (18) across the section (Σ) and under a sinusoidal pulsed regime, we obtain:

$$-\frac{\partial P}{\partial z} = \frac{2\,\mu}{\bar{\rho}\,S^2\,a}\,[\varphi]^{-1}\,\dot{M} \tag{37}$$

with

$$\varphi = \sum_{i=1}^{\infty} \frac{a\,\sin^2(b_i)}{b_i^2\,(1 + \Phi\,\sin^2(b_i))\,(b_i^2 + j\,\omega_r)^{3/2}}\,\chi_i \tag{38}$$

and

$$\chi_i = \frac{\sqrt{(b_i^2 + j\,\omega_r)}}{a} - \frac{\tanh\left(\frac{\sqrt{b_i^2 + j\,\omega_r}}{a}\right)}{1 + \Phi\,\sqrt{b_i^2 + j\,\omega_r}\,\tanh\left(\sqrt{\frac{b_i^2 + j\,\omega_r}{a}}\right)}. \tag{39}$$

Then, we may define:

$$\frac{\partial \dot{M}}{\partial z} = -IP, \qquad \frac{\partial P}{\partial z} = -J\dot{M}, \tag{40a, b}$$

with

$$J = \frac{2\mu}{\bar{\rho} S^2 a} [\varphi]^{-1}, \qquad I = j\omega \frac{S}{r\bar{\tau}\gamma} [\gamma - 2j\sigma\omega_r (\gamma - 1)\psi], \tag{41a, b}$$

where

$$\psi = \sum_{i=1}^{\infty} \frac{a \sin^2 (c_i)}{c_i^2 (1 + \phi \sin^2 (c_i)) (c_i^2 + j\omega_r \sigma)^{3/2}} \theta_i, \tag{42}$$

with

$$\theta_i = \frac{\sqrt{(c_i^2 + j\omega_r \sigma)}}{a} - \frac{\tanh\left(\frac{\sqrt{c_i^2 + j\omega_r \sigma}}{a}\right)}{1 + \phi\sqrt{c_i^2 + j\omega_r \sigma}\, \tanh\left(\sqrt{\frac{c_i^2 + j\omega_r \sigma}{a}}\right)}. \tag{43}$$

Introducing

$$\beta = \sqrt{JI}, \qquad \eta = \sqrt{\frac{J}{I}}, \tag{44}$$

the solution of system (40) may be written in the matrix form:

$$\begin{bmatrix} P_e \\ \dot{M}_e \end{bmatrix} = \begin{bmatrix} \cosh(\beta L) & \eta \sinh(\beta L) \\ \frac{\sinh(\beta L)}{\eta} & \cosh(\beta L) \end{bmatrix} \begin{bmatrix} P_s \\ \dot{M}_s \end{bmatrix}, \tag{45}$$

where the variables β and η denote the propagation factor and the characteristic impedance of the line respectively.

4.2. Analysis

As an illustration, we consider the simple case of a line closed at its outlet by a rigid wall. The outlet instantaneous mass flow rate is thus equal to zero ($\dot{M}_s = 0$).

Eq. (45) represents the solution of system (40). It allows to relate the inlet pressure and mass flow rate complex amplitudes to the outlet pressure and mass flow rate complex amplitudes. But it is also possible to determine the mass flow rate complex amplitude within any cross-section of the line by writing Eq. (45) between the inlet section ($z = 0$) and a current section (z). So, the influence of slip on the mass flow rate complex amplitude may be expressed as:

$$\frac{\dot{M}_{ns}}{\dot{M}} = \frac{\frac{\tanh(\beta_{ns} L)}{\eta_{ns}} \cosh(\beta_{ns} z) - \frac{\sinh(\beta_{ns} z)}{\eta_{ns}}}{\frac{\tanh(\beta L)}{\eta} \cosh(\beta z) - \frac{\sinh(\beta z)}{\eta}}, \tag{46}$$

where $\dot{M}_{ns}$ denotes the mass flow rate amplitude when the slip is not taken into account. The parameters β_{ns} and η_{ns} can be computed from Eq. (44) where $K = 0$. The modulus of Eq. (46) is denoted by $\dot{M}^*$.

Figure 4 represents the variation of the ratio $\dot{M}^*$ as a function of the parameter z^*. The line considered has a square cross-section which is .62 μm deep and 1 mm long. The Knudsen number is equal to .1. Whatever the position z^* of the section, the amplitude of the fluctuating mass flow rate is underestimated when slip at the walls is not taken into account. The relative influence of slip is all the more important since the considered section is far from the inlet. Because the fluctuating mass flow rate amplitude reaches a maximum for a frequency which is different whether slip is taken into account or not, the sign of the gradient $\frac{\partial \dot{M}^*}{\partial \omega_r}$ may change in the frequency range considered, as is the case for curve (1) in Figure 4.

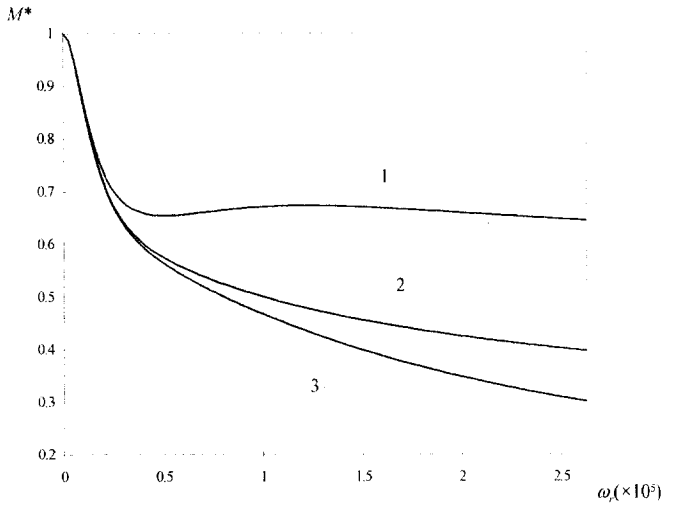

Fig. 4. – Influence of slip on the mass rate amplitude within a current section (z^*). $a = 1$, $2h = .62$ μm, $L = 1$ mm, $\bar{\tau} = 293$ K, $\bar{p} = .11$ MPa. **1** $z^* = 1/8$, **2** $z^* = 1/2$, **3** $z^* = 3/4$.

On the other hand, the ratio of the inlet complex pressure to the outlet complex pressure amplitudes can be obtained from Eq. (45) as:

$$\frac{P_s}{P_e} = \frac{1}{\cosh(\beta L)}. \tag{47}$$

As our interest lies more in the ratio of the outlet over inlet pressure amplitude, the modulus of Eq. (47) is used. This ratio is denoted by

$$P^* = \left| \frac{P_s}{P_e} \right| . \tag{48}$$

At the inlet of the microchannel, a sinusoidal pressure variation in generated. At the outlet, we obtain an out of phase signal at the same frequency but of a different amplitude. We consider a band pass at -3 dB, *i.e.* a frequency range for which the ratio P^* of the

pressure amplitudes is up to $\frac{1}{\sqrt{2}} \approx .7$. The mean temperature $\bar{\tau}$ and pressure $\bar{p}$ have a value of 293 K and .11 MPa respectively.

Figures 5, 6 and 7 respectively emphasize the role of the length L of the line, the area S and the aspect ratio a of the cross-section (Σ) on the band pass. The ratio of the band pass with slip over the band pass without slip at the wall is denoted by δ. By not taking into account slip at the walls, the band pass is underestimated whatever case is chosen. Note first that the frequency ω appears in a dimensionless form ω_r in Figure 5, but not in Figures 6 and 7. This is due to the fact that ω_r depends on the depth $2h$ of the channel. So, a comparison of curves for which $2h$ varies (*Fig.* 6 and 7) as a function of ω_r, would be devoid of interest.

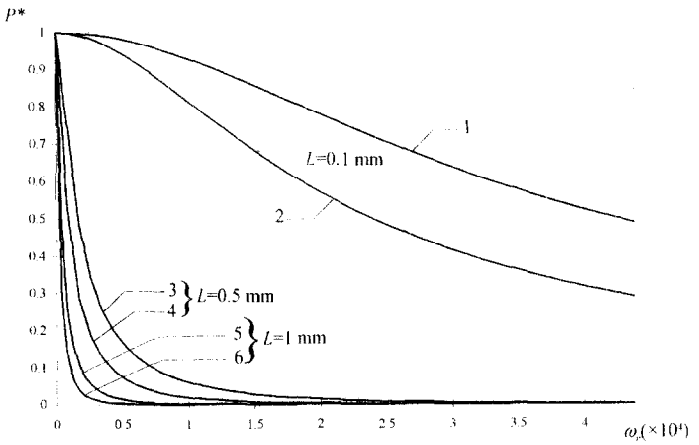

Fig. 5. – Influence of length L on the outlet over inlet pressure ratio P^* for a square line closed at its outlet end. $2h = .62$ μm, $\bar{\tau} = 293$ K, $\bar{p} = .11$ MPa. $L = .1$ mm: **1** slip flow, **2** no-slip flow. $L = .5$ mm: **3** slip flow, **4** no-slip flow. $L = 1$ mm: **5** slip flow, **6** no-slip flow.

Figure 5 represents the ratio P^* as a function of ω_r for different values of the length L. The line in question has a square cross-section and is .62 μm deep. The Knudsen number is equal to .1. We notice that the decrease in length obviously leads the band pass to increase whether slip is taken into account or not. In addition, whatever the length of the duct, the ratio δ of the band pass with and without slip is almost constant. Indeed, the computation of the ratio δ comes down to the following equation:

$$\frac{1}{\cosh(\beta L)} = \text{constant} \approx .7. \tag{49}$$

But the propagation factor β is a function of the frequency f and the Knudsen number. From Eq. (44) β may thus be written as follows:

$$\beta = \sqrt{2 j \pi f \frac{2\mu}{\bar{\rho} r \bar{\tau} S a \gamma} \frac{\gamma - 2\sigma j \omega_r (\gamma - 1)\psi}{\varphi}}, \tag{50}$$

where ψ and φ are two functions of ω_r and so of the frequency f. These functions ψ and φ are respectively expressed by Eqs. (42) and (38). For the conditions of Figure 5,

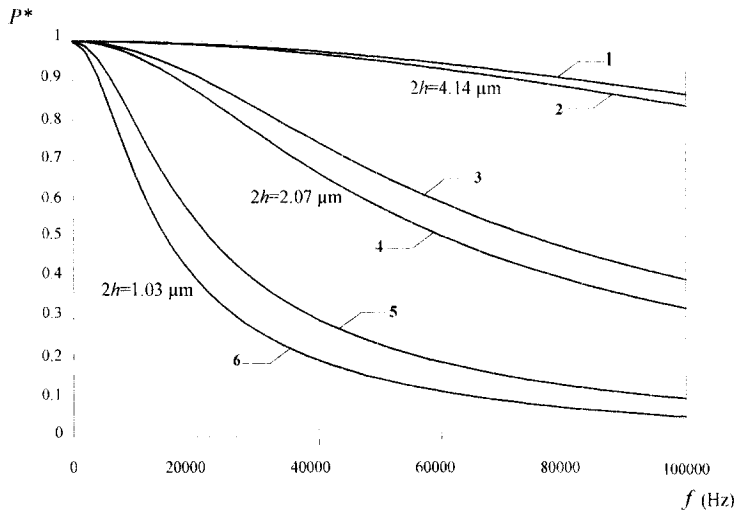

Fig. 6. – Influence of cross-sectional depth $2h$ on the outlet over inlet pressure ratio P^* for a square line closed at its outlet end. $L = 100\,\mu$m, $\bar{\tau} = 293$ K, $\bar{p} = .11$ MPa. $2h = 4.14\,\mu$m: **1** slip flow, **2** no-slip flow. $2h = 2.07\,\mu$m: **3** slip flow, **4** no-slip flow. $2h = 1.03\,\mu$m: **5** slip flow, **6** no-slip flow.

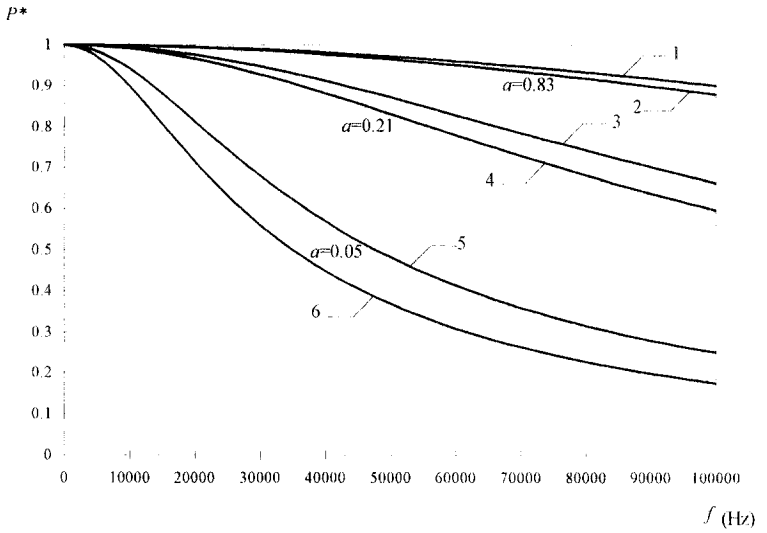

Fig. 7. – Influence of aspect ratio a on the outlet over inlet pressure ratio P^* for a line closed at its outlet end. $S = 20.698\,\mu$m^2, $L = 100\,\mu$m, $\bar{\tau} = 293$ K, $\bar{p} = .11$ MPa. $a = .83$: **1** slip flow, **2** no-slip flow. $a = .21$: **3** slip flow, **4** no-slip flow. $a = .05$: **5** slip flow, **6** no-slip flow.

the two parameters

$$\varepsilon_1 = \frac{j\,\omega_r}{b_i^2}, \qquad \varepsilon_2 = \frac{j\,\omega_r}{c_i^2} \tag{51}$$

take infinitely small values. So, in a first approximation, β appears to be the product of two functions:

$$\beta(f,\, Kn) \approx \sqrt{f}\,\Psi(Kn) \tag{52}$$

where Ψ is only dependent on the Knudsen number. If the only positive solution of Eq. (49) is denoted by β_0, we obtain:

$$\sqrt{f} \approx \frac{\beta_0}{\Psi(Kn)}, \tag{53}$$

and

$$\sqrt{\delta} \approx \frac{\Psi(0)}{\Psi(Kn)}, \tag{54}$$

where δ represents the ratio of the band pass when taking into account slip at the walls or not, for the same length L of the duct. As a result, the ratio δ is independent of the length L of the duct in a first approximation.

Figure 6 represents the evolution of the ratio P^* as a function of f for different depths $2h$ with a fixed aspect ratio $a = 1$. We logically notice that the band pass decreases when the area S of the cross-section decreases whether slip is taken into account or not. We also confirm that the more the area S decreases, the more the no-slip model is incorrect, for the role of slip increases.

The pressure ratio P^* is plotted in Figure 7 as a function of the aspect ratio. The line in question has an area $S = 20.698\ \mu\text{m}^2$ and a length $L = 100\ \mu\text{m}$. Whether slip at the walls is taken into account or not, as the aspect ratio a increases (*i.e.* as the cross-section gets closer to a square cross-section), the band pass increases, since the hydraulic diameter increases. Likewise, with a uniform area, the ratio decreases as the wall effects become less significant.

In short, the present analysis of the pneumatic line frequency response has demonstrated several results. By not taking into account slip at the walls, the band pass is underestimated. It can be also noted that the ratio δ, which represents the influence of slip on the band pass, depends not only on the Knudsen number but also on the pair $(2h,\ a)$. Different values of δ for the same Knudsen number can thus be obtained. Furthermore, the search for possible resonances shows that they only occur within a frequency range (of the order of 10^8 Hz) which is not encountered in microsystems, whilst, for lines with cross-dimensions of the order of one millimeter, this trend appears at much lower frequencies. It can finally be observed that the band pass as well as the instantaneous velocity profiles behave similarly in circular ducts (Caen *et al.*, 1996).

5. Connection of two lines in series

In order to model a fluid microsystem which connects several microchannels of different sizes, it is appropriate to model in the first place the behavior of two pneumatic lines in series.

5.1. Modeling

The lengths of the ducts in question are sufficiently larger than the transverse dimensions and the flow rate sufficiently weak for the effects of a sudden expansion to be very localized and the flow to remain parallel along the two lines. Under these assumptions, the expression for the frequency response of one microline can be applied to model the frequency response of two uniform microlines in series.

Eq. (45) allows to connect together the variables P_e, $\dot{M}_e$, P_s, $\dot{M}_s$ of a line with uniform cross-section. In the case of two lines (*Fig.* 8), the preceding variables can be connected as follows:

(55)
$$\begin{bmatrix} P_e \\ \dot{M}_e \end{bmatrix} = \begin{bmatrix} \cosh(\beta_2 L_2) & \eta_2 \sinh(\beta_2 L_2) \\ \dfrac{\sinh(\beta_2 L_2)}{\eta_2} & \cosh(\beta_2 L_2) \end{bmatrix} \begin{bmatrix} \cosh(\beta_1 L_1) & \eta_1 \sinh(\beta_1 L_1) \\ \dfrac{\sinh(\beta_1 L_1)}{\eta_1} & \cosh(\beta_1 L_1) \end{bmatrix} \begin{bmatrix} P_s \\ \dot{M}_s \end{bmatrix},$$

with

(56)
$$\beta_1 = \sqrt{J_1 I_1}, \qquad \eta_1 = \sqrt{\frac{J_1}{I_1}},$$

and

(57)
$$\beta_2 = \sqrt{J_2 I_2}, \qquad \eta_2 = \sqrt{\frac{J_2}{I_2}},$$

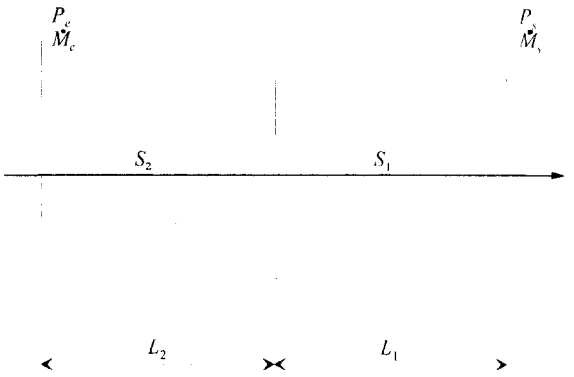

Fig. 8. – Connecting of two lines in series.

The aforementioned variables β and η are computed from Eqs. (41a) and (41b). In the case where the second line is closed at its outlet, we obtain:

(58)
$$\frac{P_s}{P_e} = \frac{2}{\left(1 + \frac{\eta_2}{\eta_1}\right)\cosh(\beta_1 L_1 + \beta_2 L_2) + \left(1 - \frac{\eta_2}{\eta_1}\right)\cosh(\beta_1 L_1 - \beta_2 L_2)}$$

5.2. Analysis

Of particular interest is the ratio P^* of the outlet to the inlet pressure amplitude, which is the modulus of Eq. (58).

As in the previous section, it can be seen that by not taking into account slip at the walls, the band pass of the line is underestimated. According to the preceding results, the band pass increases when the length of one or two ducts decreases.

In Figure 9, the significance of the site of the pressure generating system is underlined. In case 1, the fluid medium is excited at the inlet of the smallest cross-section duct, the other being closed at its outlet. In case 2, the fluid medium is excited at the inlet of the largest cross-section duct, the other being closed at its outlet. It can be noticed that the band pass is more significant in case 2.

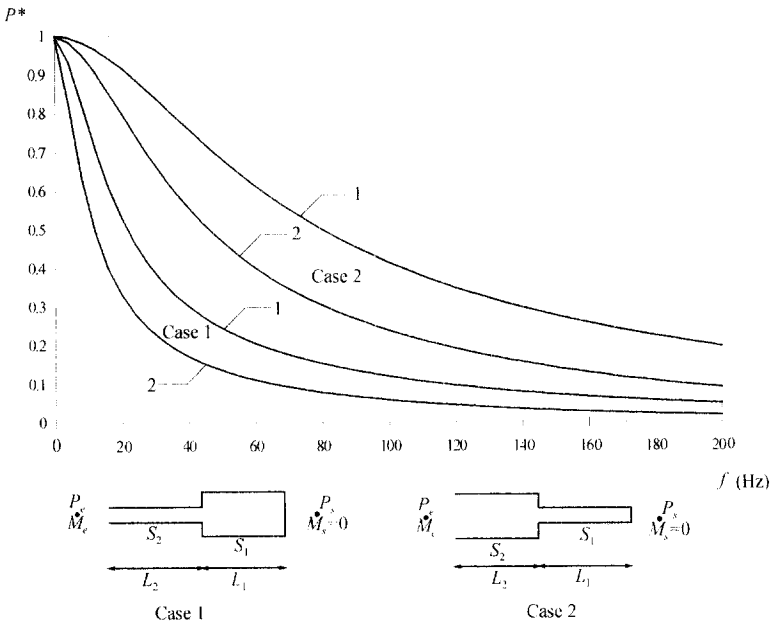

Fig. 9. – Connecting of two lines in series. Influence of the site of pressure generating system. $S_2 = .38\ \mu m^2$, $S_1 = 1.07\ \mu m^2$, $a_2 = a_1 = 1$, $L_2 = 1$ mm, $L_1 = .5$ mm, $\bar{\tau} = 293$ K, $\bar{p} = .11$ MPa. Case1: **1** slip flow, **2** no-slip flow. Case 2: **1** slip flow, **2** no-slip flow.

In this modeling of two lines in series, the singular pressure drop which is due to the sudden expansion is neglected with respect to the distributed pressure drop. This is justified because of the small Reynolds numbers. If the band pass is greater in case 2, this is also essentially due to a greater energy supply since the inlet cross-section area is larger than in case 1. Finally, by not taking into account slip at the walls, the asymmetry of the behavior between the two cases 1 and 2 is overestimated. In other words, the ratio of the band pass in case 2 over the band pass in case 1 is overestimated.

5.3. Practical implications

Not only can the tool that has been presented here help in the modeling and improvement of fluid microsystems, it can also enable us to envision the feasibility of experimental pressure measurements in an unsteady regime. Indeed, for a given pressure sensor with known dimensions and volumetric variation, the limitations of use may be determined according to its site. First of all, it must be stated that a pressure sensor cannot at the moment be placed directly in a microchannel; as the displacement of the pressure sensor diaphragm is of the order of the microchannel depth (10^{-6} m), the measurement would significantly disturb the flow. In the steady regime, the solution to this problem consists in connecting several pressure sensors to the microchannel through very small bridging channels (Pong *et al.*, 1994). Whether such pressure sensors can be used for measurements in unsteady flow and how they must be placed with regard to the microchannel remains an open issue.

For example, consider a pressure sensor with a 250 μm-by-250 μm diaphragm (as in the case of pressure sensors used by Pong *et al.* (1994)). With this pressure sensor, it is hoped to measure the pressure signal at the outlet of a line under a pulsed sinusoidal regime. The line in question is 2 μm deep, 50 μm wide and 1 mm long.

In the first layout (*Fig.* 10), the pressure sensor is perpendicular to the flow and is placed at the end of a second line mounted in series. This line is 250 μm wide, 250 μm deep and 2 mm long. In a second layout (*Fig.* 11), the sensor is placed on the lower side of a second line connected in series. This line is 250 μm wide, 10 μm deep and 2 mm long. Schematic views of the ducts are not scale drawings.

In the first layout, the signal appears to be greatly lessened but corresponds to an accurate measurement of pressure P_s within the end cross-section of the duct. In the

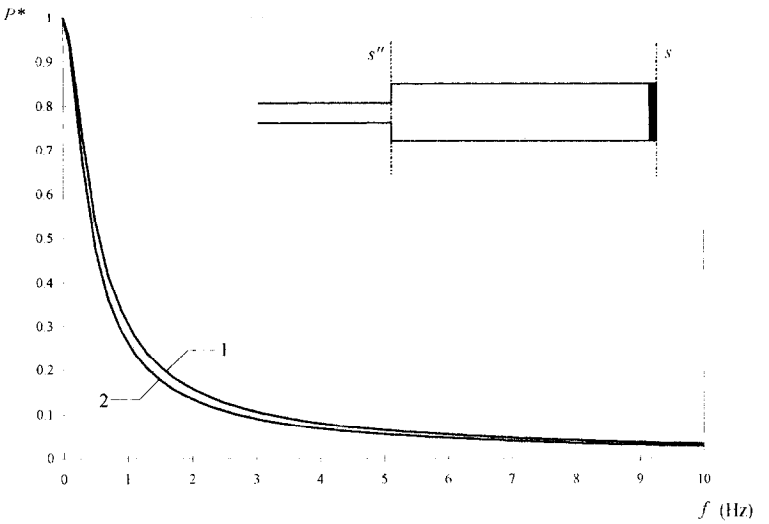

Fig. 10. – Pressure sensor. First layout. $S_2 = 1.03 \cdot 10^{-10}$ m^2, $S_1 = 625 \cdot 10^{-10}$ m^2, $a_2 = .0414$, $a_1 = 1$, $L_2 = 1$ mm, $L_1 = 2$ mm, $\bar{\tau} = 293$ K, $\bar{p} = .11$ MPa. **1** slip flow, **2** no-slip flow.

second layout, the signal is much larger. But according to the dimensions of the diaphragm, it now corresponds to a mean pressure measurement between the cross-sections s' and s. Consequently, this measurement is less accurate than that of the previous case.

From the measurements given by the pressure sensor in layout one (*Fig.* 10) or two (*Fig.* 11) and with the help of the present theoretical model, we can deduce the pressure signal within the end cross-section s'' of the microchannel, provided that the volumetric variation of the sensor has a negligible influence. This gives an accurate enough idea of this influence: the volume $\Delta\vartheta$ displaced by the sensor is compared to the volumetric variation ΔV of the gas in the duct, under a pressure variation ΔP and during an isothermal process. Thus, we have:

$$\frac{\Delta V}{\Delta P} = \frac{S_2 L_2 + S_1 L_1}{\bar{p}}. \tag{59}$$

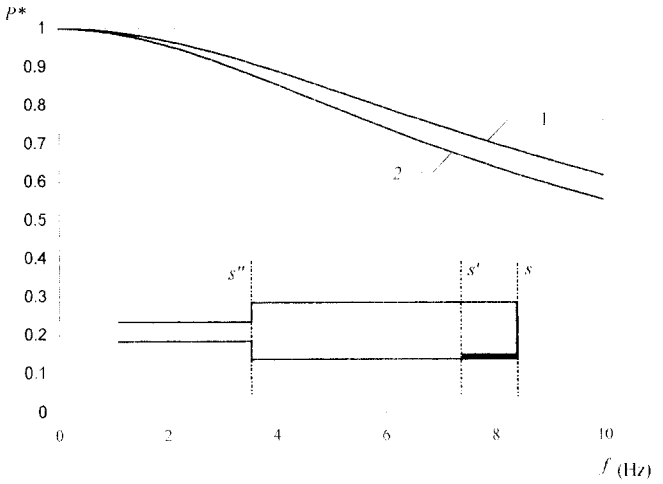

Fig. 11. – Pressure sensor. Second layout. $S_2 = 1.03 \cdot 10^{-10}$ m^2, $S_1 = 25 \cdot 10^{-10}$ m^2, $a_2 = .0414$, $a_1 = .04$, $L_2 = 1$ mm, $L_1 = 2$ mm, $\bar{\tau} = 293$ K, $\bar{p} = .11$ MPa. **1** slip flow, **2** no-slip flow.

Now, suppose that the sensor in question has a diaphragm with a mean displacement of 1 μm under a pressure variation $\Delta P = 10^4$ Pa. We have thus $\frac{\Delta\vartheta}{\Delta P} \approx 6.10^{-18}$ m^3 Pa^{-1}. This ratio is small with respect to $\frac{\Delta V}{\Delta P}$ (layout 1) $\approx 1.10^{-15}$ m^3 Pa^{-1} but it begins to become significant with respect to $\frac{\Delta V}{\Delta P}$ (layout 2) $\approx 5.10^{-17}$ m^3 Pa^{-1}.

In conclusion, in order to make pressure measurements in an unsteady flow without disturbing the flow, one may place the pressure sensor in a second line mounted in series. With current dimensions for the smallest sensors, two sensor sites are proposed. In the first case, the signal is significantly reduced, so the sensors must be able to measure very low pressure variations. In the other case, the signal is larger but the measured pressure is not a local pressure.

6. Conclusion

A first model of an unsteady gaseous flow in rectangular microchannels has been presented. The aim has been to demonstrate the influence of slip on the instantaneous velocity profiles and on the frequency response of one and two microlines in series.

According to the results based on the steady regime, by not taking into account slip at the walls, the instantaneous mass flow rate is underestimated. As regards the frequency response of one or two pneumatic microlines, the band pass is also underestimated when slip is not taken into account. Finally, although a pressure sensor may not be placed directly in the microchannel as yet, this investigation allows the feasibility of experimental measurements in unsteady regimes to be specified.

Acknowledgement. – We would like to thank Dr. P. Guillaume (from the Mathematical Engineering Department of INSAT, Toulouse) for his valuable assistance.

REFERENCES

ALBERTONI S., CERCIGNANI C., GOTUSSO L., 1963, Numerical evaluation of the slip coefficient., *Phys. Fluids*, **6**, 993-996.

ARKILIC E. B., BREUER K. S., 1993, Gaseous flow in small channels. *A.I.A.A.* Paper 93-3270, 1-7.

ARKILIC E. B., BREUER K. S., SCHMIDT M. A., 1994, Gaseous flow in microchannels. *A.S.M.E.* Paper, **FED-197**, 57-66.

BARRON R. F., WANG X. M., AMEEL T. A., WARRINGTON R. O., 1997, The Graetz problem extended to slip flow. *Int. J. Heat Mass Transfer*, **40**, 1817-1823.

BESKOK A., KARNIADAKIS G. E., 1994, Simulation of heat and momentum transfer in complex microgeometries. *J. Thermophys. Heat Transfer*, **8**, 647-655.

BESKOK A., KARNIADAKIS G. E., TRIMMER W., 1996, Rarefaction and compressibility effects in gas microflows. *J. Fluids Eng.*, **118**, 448-456.

BESTMAN A. R., IKONWA I. O., MBELEDOGU I. U., 1995, Transient slip flow. *Int. J. Energy Res.*, **19**, 275-277.

BOUROUINA T., GRANDCHAMP J. P., 1996, Modeling micropumps with electrical equivalent networks. *J. Micromech. Microeng.*, **6**, 398-404.

CAEN R., 1979, Contribution à l'étude des écoulements instationnaires dans les circuits pneumatiques. Applications à la réponse fréquentielle d'un amplificateur fluidique analogique. Thèse de Doctorat d'Etat. INP Toulouse.

CAEN R., MAS I., COLIN S., 1996, Ecoulements non permanents dans les microcanaux: réponse fréquentielle des microtubes pneumatiques. *C.R.A.S., Série II.b*, **323**, 805-812.

CARMONA M., MARCO S., SAMITIER J., MORANTE J. R., 1996, Dynamic simulations of micropumps. *J. Micromech. Microeng.*, **6**, 128-130.

CHOI S. B., BARRON R. F., WARRINGTON R. O., 1991, Fluid flow and heat transfer in microtubes. *A.S.M.E.* Paper, **DSC-32**, 123-133.

CHU W. K. H., 1996, Stokes slip flow between corrugated walls. *Z angew Math Phys.*, **47**, 591-599.

DEISSLER R.G., 1964, An analysis of second-order slip flow and temperature jump boundary conditions for rarefied gases. *Int. J. Heat Mass Transfer*, **7**, 681-694.

D'SOUZA A.F., OLDENBURGER, R., 1964, Dynamic response of fluid lines. *J. Basic Eng.*, 589-598.

EBERT W. A., SPARROW E. M., 1965, Slip flow in rectangular and annular ducts. *J. Basic Eng.*, **87**, 1018-1024.

FUNK J. E., ROBE T. R., 1969, Transients in pneumatic transmission lines subjected to large pressure changes. *A.S.M.E.* Paper, **69-FLCS-42**, 1-12.

GRAVESEN P., BRANEBJERG J., JENSEN O. S., 1993, Microfluidics - a review. *J. Micromech. Microeng.*, **3**, 168-182.

HARLEY J. C., HUANG Y., BAU H. H., ZEMEL J. N., 1995, Gas flow in micro-channels. *J. Fluid Mech.*, **284**, 257-274.

HEALEY A. J., CARLSON R. J., 1969, Frequency response of rectangular pneumatic transmission lines. *A.S.M.E.* Paper, **WA/FL-5**, 1-8.

KENNARD E. H., 1938, Kinetic theory of gases. *McGraw-Hill Book Company*, New York.

MALA G. M., LI D. Q., DALE J. D., 1997, Heat transfer and fluid flow in microchannels. *Int. J. Heat Mass Transfer*, **40**, 3079-3088.

MUNTZ E. P., 1989, Rarefied gas dynamics. *Ann. Rev. Fluid Mech.*, **21**, 387-417.

NICHOLS N. B., 1962, The linear properties of pneumatic transmission lines. *I.S.A. Transactions*, **1**, 5-14.

NORBERG P., ACKELID U., LUNDSTRÖM I., PETERSON L. G., 1997, On the transient gas flow through catalytically active micromachined channels. *J. Appl. Phys.*, **81** (5), 2094-2100.

PFAHLER J., HARLEY J., BAU H., ZEMEL, J., 1991, Gas and liquid flow in small channels. *A.S.M.E.* Paper, **DSC-32**, 49-60.

PIEKOS E. S., BREUER K. S., 1996, Numerical modeling of micromechanical devices using the direct simulation Monte Carlo method. *J. Fluid Eng.*, **118**, 464-469.

PONG K. C., HO C. M., LIU J., TAI Y. C., 1994, Non-linear pressure distribution in uniform microchannels. *A.S.M.E.* Paper, **FED-197**, 51-56.

SCHAAF S. A., 1963, Mechanics of Rarefied Gases. *In Encyclopedia of Physics*, Berlin, Fluid Dynamics II, **VII/2**, 591-624.

SCHAEDEL H., 1968, A theoretical investigation of fluidic transmission lines with rectangular cross section. *Third Cranfield Fluidics Conference*, Turin, **K3**, 33-52.

SCHOMBURG W. K., VOLLMER J., BUSTGENS B., FAHRENBERG J., HEIN H., MENZ W., 1994, Microfluidic components in LIGA technique. *J. Micromech. Microeng.*, **4**, 186-191.

SHOJI S., ESASHI M., 1994, Microflow devices and systems. *J. Micromech. Microeng.*, **4**, 157-171.

SONE Y., WANIGUCHI Y., AOKI K., 1996, One-way flow of a rarefied gas induced in a channel with a periodic temperature distribution. *Phys. Fluids*, **8**, 2227-2235.

SREEKANTH A. K., 1968, Slip flow through long circular tubes. *In 6th International Symposium on Rarefied Gas Dynamics*. Ed. L. Trilling and H.Y. Wachman, Academic Press, New York, M.I.T., 667-680.

STEFANOV S., CERCIGNANI C., 1994, Monte Carlo simulation of a channel flow of a rarefied gas. *Eur. J. Mech. B /Fluids*, **13**, 93-114.

SUGIYAMA W., SAWADA T., NAKAMORI K., 1996, Rarefied gas flow between two flat plates with two dimensional surface roughness. *Vacuum*, **47**, 791-794.

THOMSON S. L., OWENS W. R., 1975, A survey of flow at low pressures. *Vacuum*, **25**, 151-156.

TISON S. A., 1993, Experimental data and theoretical modeling of gas flows through metal capillary leaks. *Vacuum*, **44**, 1171-1175.

VAN DE POL F. C. M., BRANEBJERG J., 1990, Micro liquid-handling devices - A review, *MST*, Berlin, 799-805.

WHITE F. M., 1991, Viscous fluid flow. *Mac Graw-Hill International Editions*, New York.

ZENGERLE R., RICHTER M., 1994, Simulation of microfluid systems. *J. Micromech. Microeng.*, **4**, 192-204.

(Manuscript received September 19, 1996;
revised July 2, 1997;
accepted September 4, 1997.)